Time-dependent shot noise in multi-level quantum dot-based single-electron devices

V Talbo[1], J Mateos[1], S Retailleau[2], P Dollfus[2] and T González[1]

[1] Departamento de Física Aplicada, Universidad de Salamanca, Plaza de la Merced s/n, E-37008 Salamanca, Spain
[2] Institut d'Electronique Fondamentale, Université Paris-Sud, CNRS UMR 8622, F-91405 Orsay, France

E-mail: vtalbo@usal.es

CrossMark

Abstract

By means of three-dimensional self-consistent simulation, we investigate the time- and frequency-dependent shot noise in multi-level quantum dot (QD)-based double-tunnel junction by analyzing auto-correlation functions and distribution of waiting times between consecutive tunnel events through a given barrier. We derive analytic expressions for correlation and waiting time distributions (WTDs) in the case of a maximum of two electrons in the QD. We separate the contributions of the different evolution paths of the number of electrons in the dot between two consecutive current pulses, called 'basic paths'. The close relation revealed between probabilities, WTDs and correlation functions associated to basic paths allows a good understanding of the specific dynamics in spectral densities. The analytic results show a perfect agreement with those obtained from numerical Monte-Carlo simulation.

Keywords: single-electron devices, shot noise, Monte-Carlo simulation, double-tunnel junction

(Some figures may appear in colour only in the online journal)

1. Introduction

With the advent of solid-state mesoscopic and nanoscale systems controlled by a small amount of electrons, shot noise (SN), as a direct consequence of the discreteness of electronic charge, has been intensively studied over the last decades, providing complementary information about electronic transport to that given by the conductance measurements [1–6]. In the case of uncorrelated processes, the transport is Poissonian. The spectral density $S(\omega)$ related to SN is then often characterized at low frequency by its deviation to fully Poissonian SN $2e\langle I \rangle$, where $\langle I \rangle$ is the mean current, and the Fano factor is defined as the ratio $F = S(0)/2e\langle I \rangle$.

Single-electron devices, and in particular single-electron transistors (SETs), are of great interest in nanotechnology. If the ability of SET to provide a fine control of current due to Coulomb blockade is known since the late 1980s [7–10], it is only recently that experimental Silicon quantum dot (QD)-based SETs, likely to be integrated in silicon electronics, have shown good Coulomb-blockade oscillations at room temperature [11–15]. In the meantime, detection of single-electron events in devices has been performed experimentally,

allowing measurements of SN and higher order correlation functions, mostly using a quantum point contact [16–32].

Most of these studies have been interpreted in the framework of the full counting statistics tool, developed by Levitov and Lesovik [33, 34], determining the probability distributions of electrons transferred during long time, giving access to all zero-frequency current-correlation functions. This theory has been extended to Coulomb blockade regime [35]. Previously, a formalism developed by Korotkov provided expressions for both static and frequency dependent SN in single-electron devices, depending on the tunnel transfer rates and the number of electrons in the QD [36]. Thanks to those tools, we are able to understand the behavior of zero-frequency SN, its suppression down to a sub-Poissonian Fano factor $F = 0.5$ in a single-level QD where in and out tunnel transfer rates are equal [37, 38], or its enhancement up to super-Poissonian noise due to multi-levels in QDs [39], lifting of spin degeneracy [40–42] or inelastic cotunneling regime [43].

Although the calculation of finite frequency behavior of SN has been demonstrated [30, 44, 45], an alternative method has emerged recently, focusing on the time-domain. By

studying the distribution of time-delay between two consecutive tunnel events, the electron waiting time distribution (WTD) tool provides useful information about the short-time physics in single-electron transport [46–56].

About a decade ago, a 3D simulator, called single-electron nanodevice simulation (SENS) was developed to study single-electron devices with geometry and bias as input data [57, 58]. It relies on a 3D solver of Poisson and Schrödinger coupled equations, reaching wave-functions for each electron in the dot, then allowing the calculation of tunnel transfer rates depending on the number of electrons in the QD. Initially developed for the evaluation of *I–V* characteristics in double-tunnel junctions (DTJs) [57], it has been extended to double-dot structures by introducing phonon contribution [59] and SETs by including the effect of a gate [60]. In a previous article [61], we used Korotkov's formula to calculate zero-frequency SN in a Si-QD based DTJ, explaining sub and super-Poissonian regimes through a comparison of tunnel transfer rates. The simulator also stands on a Monte-Carlo (MC) algorithm to follow the time-evolution of the number of electrons in QDs, giving access to all the time-dependent characteristics of the current, paving the way for the simulation of complex structures for which an analytic formalism could be difficult to find out.

In this paper, on the basis of tunneling rates calculated using the code SENS, we investigate the frequency-dependent SN in an Si-based DTJ within Korotkov formalism, limiting ourselves to a 3-state case (0-1-2 electrons in the QD). As a novelty here, we introduce the notion of basic paths, representing the different possible evolution paths of the number of electrons in the QD between two consecutive tunnel events through source oxide. The WTD, cross- and auto-correlations related to each basic path are determined. The close link between WTD and correlation functions, and the study of the contribution of each basic path give a clear and intuitive explanation of the overall frequency-dependent SN. A successful comparison between analytic results and MC simulations is also provided.

The paper is organized as follows. In section 2, the models used in the code SENS and the formalism for frequency-dependent correlations and WTD are briefly presented. The resulting zero-frequency and frequency-dependent SN for different bias conditions and values of Fano factor are analyzed in section 3 in terms of basic paths and WTDs.

2. Model

2.1. The code SENS

The models used in the code SENS to simulate QD-based single-electron structures have been widely described in the case of simulation of DTJs [57, 58], double-dot structures [59] and SETs [60]. Here, we summarize the main stages of the calculation for an Si-QD based DTJ, as schematized on figure 1.
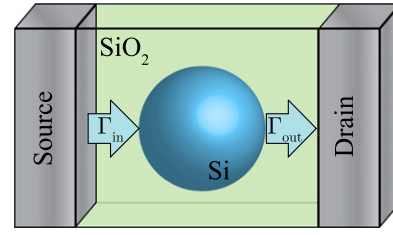

Figure 1. Schematic view of a double-tunnel junction.

The simulator relies on three stages. First, the 3D Poisson–Schrödinger coupled equations are self-consistently solved to calculate the electronic structure in the QD, depending on the bias voltage, within effective mass and Hartree approximations, proven to be correct for Si-QDs of radius greater than 1.5 nm [62, 63]. Thanks to the Hartree method, the wave-function ψ_i and the energy level μ_i are provided for each electron i in the dot.

Those wave functions are then used to calculate the tunneling rates between the lead L and the dot d containing N electrons from the Fermi golden rule (weak coupling limit) as

$$\begin{cases} \Gamma_{\mathrm{Ld}}(N) = \dfrac{2\pi}{\hbar} \, |M(N+1)|^2 \rho_L \; l_N \; f_L\left(\mu_{N+1}, T_L\right), \\ \Gamma_{\mathrm{dL}}(N) = \dfrac{2\pi}{\hbar} \, |M(N)|^2 \rho_L \; g_N \left[1 - f_L\left(\mu_N, T_L\right)\right], \end{cases} \quad (1)$$

where g_N, l_N, T_L, $f_L(\mu_L, T_L)$, and ρ_L are the number of electrons on the energy level μ_L, the number of free states on this level, the temperature of the lead, the Fermi function of the lead and the density of states of the lead, respectively. The tunneling matrix element M is given by the Bardeen formula [58, 64].

Finally, the tunnel transfer rates are used to calculate the electrical characteristics of the device. Two methods can be used. First, from the master equation, we can deduce the static probabilities of having N electrons in the dot $P_{t=\infty}(N)$, and then the mean current is given by

$$\langle I \rangle = e \sum_N P_{t=\infty}(N)\left[\Gamma_{\mathrm{Sd}}(N) - \Gamma_{\mathrm{dS}}(N)\right]. \quad (2)$$

The Fano factor, current auto-correlation function and spectral density are obtained using Korotkov formalism (equations (35), (18) and (28) in [36], respectively). The method consists mainly in the determination of the auto-correlation function by calculating the probability P_{t_1,t_2} to have two tunnel events through a given junction (in this paper, the source one) at times t_1 and $t_2 > t_1$, i.e.

$$\begin{aligned} P_{t_1,t_2} = & \; \Gamma_{\mathrm{Sd}}(N_2)\mathrm{d}t_2 P_{t=t_2-t_1}\left(N_2|N_1+1\right) \\ & \times \Gamma_{\mathrm{Sd}}(N_1)\mathrm{d}t_1 P_{t=\infty}(N_1), \end{aligned} \quad (3)$$

where $N_1 = N(t_1)$, $N_2 = N(t_2)$ (before the tunnel event) and $P_{t=\tau}(N|N')$ is the time-dependent probability of having N electrons in the dot at $t = \tau$ if N′ electrons were present at $t = 0$, and is determined from the master equation. The auto-correlation function is then obtained by summing over all N_1 and N_2. The spectral density and Fano factor are deduced by a Fourier transform of the auto-correlation function.
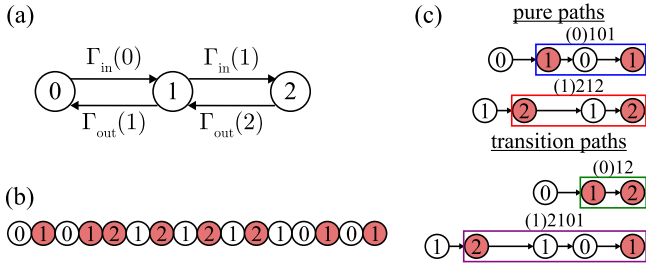
Figure 2. Schematic description of (a) all possible transitions in a 3-state case, (b) a random time-evolution of the number of electrons in the dot and (c) basic paths followed by the number of electrons in the dot between two consecutive tunnel events though source oxide. The numbers in circles are the number of electrons in the dot, in red after a tunnel event through source oxide.

Equivalently, a MC algorithm with tunnel transfer rates as input data allows us to follow the time evolution of the number of electrons in the dot, and then calculate all correlations and spectral densities.

This code is thus able to simulate and calculate static and frequency-dependent electrical characteristics in any QD-based single-electron device. However, if the behavior of single-electron currents are now well understood [57, 60], the physics of SN is more complex in multi-level QDs due to the multiple correlations between levels. This work is dedicated to the analysis of this physics.

2.2. 3-state case

In this study, we use the values of tunnel transfer rates obtained from SENS, but for the sake of simplicity we restrict ourselves to a 3-state case (only states with 0, 1 or 2 electrons in the QD are possible), i.e. with $\Gamma_{Sd}(2) = 0$. We have also set the temperature to zero, so that $\Gamma_{dS} = \Gamma_{Dd} = 0$. Hence, only four tunnel transfer rates need to be considered. In the rest of the paper, the subscript in Γ_{Sd} and Γ_{dD} will be changed to Γ_{in} and Γ_{out}, respectively, as schematized on figure 1.

In a 2-state case, the only time evolution of the number of electrons in the QD is 0–1-0-1-0-1-0-1...In the 3-state case, two events are possible if one electron is in the dot, as schematized on figure 2(a). Thus, an infinite number of time-evolution sequences is possible, for example the one illustrated in figure 2(b). Each of these time-evolution sequences are based on 4 basic paths describing the evolution of the number of electrons in the QD between two source-to-dot tunnel events. We call the basic paths (0)101 and (1)212 'pure paths' and the paths (1)2101 and (0)12 'transition paths', as they are making the transition between one pure path to another. The number in brackets refers to the number of electrons in the dot before the first tunnel event. These four paths are schematized in figure 2(c).

Indeed, if $\Gamma_{in}(1) > \Gamma_{out}(1)$, then the (1)212 path will be the most probable to be followed when an electron has crossed the source barrier. In the contrary case, the (0)101 will be more probable. The probability of basic paths P_{path} only depends on the ratio between $\Gamma_{in}(1)$ and $\Gamma_{out}(1)$ and

writes

$$P_{(0)101} = \Gamma_{out}^2(1)\big/\big(\Gamma_{in}(1) + \Gamma_{out}(1)\big)^2, \tag{4}$$

$$P_{(1)212} = \Gamma_{in}^2(1)\big/\big(\Gamma_{in}(1) + \Gamma_{out}(1)\big)^2, \tag{5}$$

$$P_{(1)2101} = P_{(0)12}$$

$$= \Gamma_{in}(1)\Gamma_{out}(1)\big/\big(\Gamma_{in}(1) + \Gamma_{out}(1)\big)^2. \tag{6}$$

We can also define their characteristic times t_{path} as

$$t_{(0)101} = \Gamma_1^{-1} + \Gamma_0^{-1}, \tag{7}$$

$$t_{(1)212} = \Gamma_2^{-1} + \Gamma_1^{-1}, \tag{8}$$

$$t_{(0)12} = \Gamma_1^{-1}, \tag{9}$$

$$t_{(1)2101} = \Gamma_2^{-1} + \Gamma_1^{-1} + \Gamma_0^{-1}, \tag{10}$$

where $\Gamma_0 = \Gamma_{in}(0)$, $\Gamma_1 = \Gamma_{in}(1) + \Gamma_{out}(1)$, $\Gamma_2 = \Gamma_{out}(2)$.

These characteristics times represent the mean duration of each corresponding path between two consecutive pulses, i.e. two tunneling events at the source barrier. To go further into the study of time-dependent SN, we should consider the WTD depending on the path followed between two pulses. The WTD $\mathcal{W}(\tau)$ represents the density of probability that the time between two consecutive events is τ [46, 47]. For a Poisson process with a rate parameter λ, the WTD is $\mathcal{W}(\tau) = \lambda e^{-\lambda\tau}$.

Considering that each tunnel process is Poissonian, we can calculate the WTD for each path by integrating the number of Poissonian tunnel events involved in a path (1 for (0)12, 2 for (1)212 and (0)101 and 3 for (1)2101):

$$\mathcal{W}_{(0)12}(\tau) = \Gamma_1 e^{-\Gamma_1\tau}, \tag{11}$$

$$\mathcal{W}_{(0)101}(\tau) = \frac{\Gamma_0\Gamma_1}{\Gamma_1 - \Gamma_0}\big(e^{-\Gamma_0\tau} - e^{-\Gamma_1\tau}\big), \tag{12}$$

$$\mathcal{W}_{(1)212}(\tau) = \frac{\Gamma_1\Gamma_2}{\Gamma_2 - \Gamma_1}\big(e^{-\Gamma_1\tau} - e^{-\Gamma_2\tau}\big), \tag{13}$$

$$\mathcal{W}_{(1)2101}(\tau) = \frac{\Gamma_0\Gamma_1\Gamma_2}{\Gamma_1 - \Gamma_0}$$

$$\times\left[\frac{e^{-\Gamma_0\tau} - e^{-\Gamma_2\tau}}{\Gamma_2 - \Gamma_0} - \frac{e^{-\Gamma_1\tau} - e^{-\Gamma_2\tau}}{\Gamma_2 - \Gamma_1}\right]. \tag{14}$$

The global WTD is then deduced from probabilities and WTDs

$$\mathcal{W}_{tot}(\tau) = \sum P_{path}\mathcal{W}_{path}(\tau). \tag{15}$$

The spectral density of current, used to characterize SN, is obtained through a Fourier transform of current auto-correlation function. Each peak of current is due to either a $0 \rightarrow 1$ or a $1 \rightarrow 2$ event, and the current is decomposed in two contributions, I_{01} and I_{12}. We define the auto- and cross-correlation functions of those two events as

$$C_{01-01}(\tau) = \langle I_{01}(t)I_{01}(t-\tau)\rangle - \langle I_{01}\rangle^2, \tag{16}$$

$$C_{12-12}(\tau) = \langle I_{12}(t)I_{12}(t-\tau)\rangle - \langle I_{12}\rangle^2, \tag{17}$$

$$C_{12-01}(\tau) = \langle I_{01}(t)I_{12}(t-\tau)\rangle - \langle I_{01}\rangle\langle I_{12}\rangle, \tag{18}$$

$$C_{01-12}(\tau) = \langle I_{12}(t)I_{01}(t-\tau)\rangle - \langle I_{01}\rangle\langle I_{12}\rangle. \tag{19}$$

Auto-correlations C_{01-01} and C_{12-12} are directly linked to the paths (0)101 and (1)212, respectively, while the cross-correlation C_{01-12} between $0 \to 1$ and subsequent $1 \to 2$ pulses are linked to (0)12 path (and the opposite for C_{12-01} and the (1)2101 path). Those correlations can be determined numerically from MC simulations. Analytically, we follow the method developed by Korotkov to derive the global auto-correlation function in [36] to determine the auto- and cross-correlations as

$$\begin{aligned} C_{01-01}(\tau) &= \mathrm{e}^2 P_{t=\infty}(0)\Gamma_{\mathrm{in}}^2(0)P_{t=\tau}(0|1) \\ &\quad + \mathrm{e}^2 P_{t=\infty}(0)\Gamma_{\mathrm{in}}(0)\delta(\tau) - \langle I_{01}\rangle^2, \end{aligned} \tag{20}$$

$$\begin{aligned} C_{12-12}(\tau) &= \mathrm{e}^2 P_{t=\infty}(1)\Gamma_{\mathrm{in}}^2(1)P_{t=\tau}(1|2) \\ &\quad + \mathrm{e}^2 P_{t=\infty}(1)\Gamma_{\mathrm{in}}(1)\delta(\tau) - \langle I_{12}\rangle^2, \end{aligned} \tag{21}$$

$$\begin{aligned} C_{01-12}(\tau) &= \mathrm{e}^2 P_{t=\infty}(0)\Gamma_{\mathrm{in}}(0)P_{t=\tau}(1|1)\Gamma_{\mathrm{in}}(1) \\ &\quad - \langle I_{01}\rangle\langle I_{12}\rangle, \end{aligned} \tag{22}$$

$$\begin{aligned} C_{12-01}(\tau) &= \mathrm{e}^2 P_{t=\infty}(1)\Gamma_{\mathrm{in}}(1)P_{t=\tau}(0|2)\Gamma_{\mathrm{in}}(0) \\ &\quad - \langle I_{01}\rangle\langle I_{12}\rangle. \end{aligned} \tag{23}$$

Indeed the sum of those contributions $C_{II}(\tau)$ leads to the general auto-correlation function of Korotkov.

The time dependences of WTD and correlation function are strongly related, because the time delay between two consecutive tunnel events through the source barrier is also the time lag on which these two events are correlated. Even though the correlation functions take into account all previous events, not only the one of the basic path considered in WTD, we expect a rather similar behavior of WTD and correlation function.

3. Results and discussion

The simulated DTJ consists in a 8 nm diameter Si QD, embedded in an SiO$_2$ matrix, forming tunnel barriers between the dot and two metallic leads, as schematized on figure 1. The tunnel barriers on source and drain sides are 1.2 nm and 1.8 nm thick, respectively. This asymmetry has been chosen to observe both positive (PDC) and negative differential conductance (NDC) regimes on distinct Coulomb stairs. The strong influence of the bias voltage on the wave-function localization towards the drain has been shown to be the cause of NDC in DTJ [57].

3.1. Current and SN

The current and Fano factor are both plotted in figure 3(a), in the normal case, i.e. without any limitation of the number of electrons in the dot, and in the case where we restrict ourselves to three possible states. The probabilities and characteristic times of basic paths for the maximum and the minimum of zero-frequency SN in the 3-state case are given in table 1.
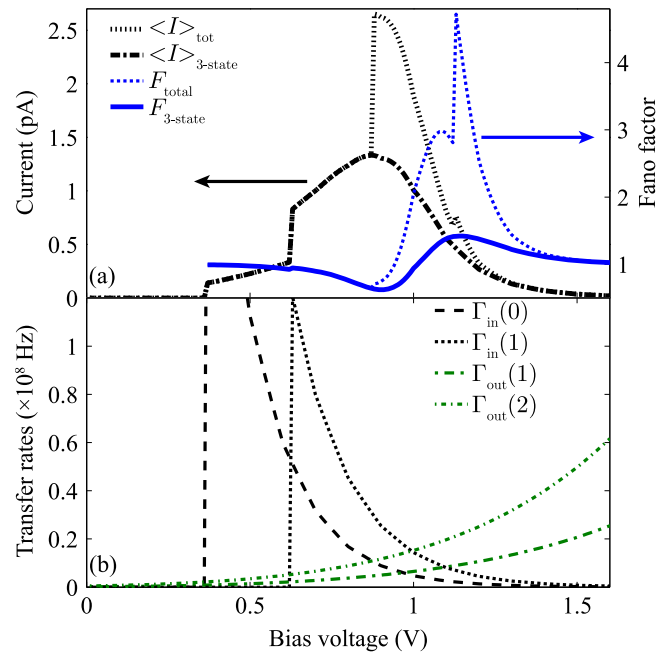

Figure 3. (a) Current and Fano factor in the normal case and the 3-state case as a function of drain voltage. (b) Tunnel transfer rates involved in the 3-state case as a function of drain voltage.

Table 1. Probabilities and characteristic times of basic paths for the extreme values of the Fano factor in the 3-state case.

basic paths	$V = 0.9$ V $F = 0.62$		$V = 1.15$ V $F = 1.42$	
	P_{path}	t_{path}	P_{path}	t_{path}
(0)101	2%	10^{-7} s	36%	6×10^{-7} s
(1)212	70%	10^{-7} s	16%	10^{-7} s
(0)12	14%	3×10^{-8} s	24%	6×10^{-8} s
(1)2101	14%	2×10^{-7} s	24%	6×10^{-7} s

In the *I–V* characteristics of the normal case, we observe two Coulomb stairs with PDC, and NDC in the following steps. In the 3-state case, the second stair shows both regimes, the NDC being a consequence of $\Gamma_{\mathrm{out}} > \Gamma_{\mathrm{in}}$, as seen on figure 3(b). On the first two steps of the normal case, the Fano factor remains sub-Poissonian, which is the typical behavior of a 2-state case [38]. In the 3-state case, the minimum of sub-Poissonian noise is $F = 0.62$ at $V = 0.9$ V. At this bias, $\Gamma_{\mathrm{in}}(1) > \Gamma_{\mathrm{out}}(1)$, promoting the (1)212 basic path up to 70%, as reported in table 1. If we were in a 2-state process (only 1 or 2 electrons in the dot), the Fano factor would be $F = 0.6$. However, the transition paths (1)2101 and (0)12 occur at a rate of 14%, with characteristic times twice longer and three times shorter than the (1)212 basic path, respectively. Thus, the (1)212 event that is 'lost' when a (1)2101 path occurs is almost compensated by a fast (0)12 event to come back to the pure sequence (1)212. As a consequence the SN value increases only slightly compared to the 2-state case.

Super-Poissonian noise is reached on the third and following stairs in the normal case, due to the increasing number of states, and thus of basic paths (8 and 13 in the 4 and 5-state cases, respectively), and, though not shown here, to the

4
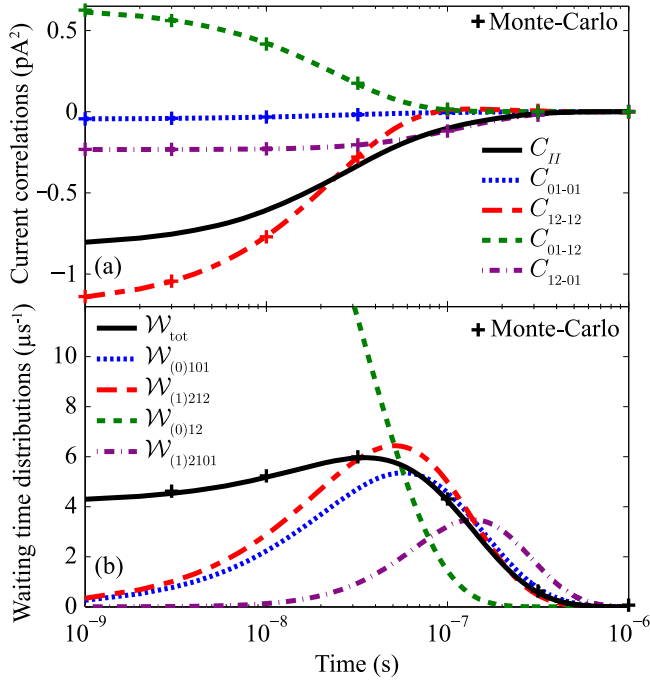
Figure 4. (a) Auto- and cross-correlations and (b) waiting time distributions corresponding to basic path and of the total current as a function of time in the case of minimum of Fano factor ($V = 0.9$ V) in the 3-state case. The lines correspond to analytic results, the crosses are the results obtained using a Monte-Carlo algorithm.
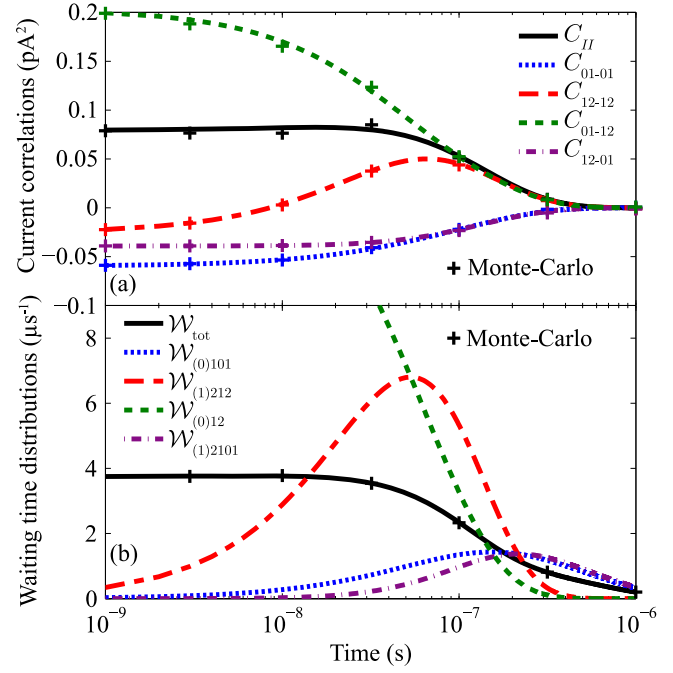

Figure 5. (a) Auto- and cross-correlations and (b) waiting time distributions corresponding to basic path and of the total current as a function of time in the case of maximum of Fano factor ($V = 1.15$ V) in the 3-state case. The lines correspond to analytic results, the crosses are the results obtained using a Monte-Carlo algorithm.

increase of probability of the transition paths. In the 3-state case, super-Poissonian noise appears around $\Gamma_{in}(1) = \Gamma_{out}(1)$, even though the maximum of SN is reached for a slightly higher bias, $F = 1.42$ at $V = 1.15$ V. The most probable basic path is then (0)101, but only with a 36% rate, the rate of transition paths being at 24%, and that of the pure path (1)212 at 16%. The (0)101 and (1)2101 paths are 6 times and 10 times longer than (1)212 and (0)12, respectively, inducing a bunching phenomenon, and then a super-Poissonian noise.

3.2. Frequency-dependent SN

The current auto- and cross-correlations ((16)–(19)) as well as WTDs ((11)–(15)) for three particular biases (minimum, maximum and nearly Poissonian Fano factor $F = 1.04$) are given in figures 4–6, respectively. For clarity reason, a logarithm scale is used for time, hiding *de facto* the zero-time values of auto-correlation functions. Those values are always positive and correspond to the variance of current, associated to the integral of the spectral densities which are shown in figure 7.

The basic path (0)12 involves only one Poissonian event, implying the maximum of WTD $\mathcal{W}_{(0)12}(\tau)$ to be located at zero. $0 \rightarrow 1$ pulses and their following $1 \rightarrow 2$ pulses are then highly correlated for low time delays, and the cross-correlations C_{01-12} are always positive, before vanishing when the correlations are lost, i.e. $\mathcal{W}_{(0)12}(\tau) \rightarrow 0$.

Conversely, we have $\mathcal{W}_{(1)212}(0) = \mathcal{W}_{(0)101}(0) = 0$ as a consequence of Coulomb blockade: one electron has to leave the dot for another to cross the source barrier. Thus, it is
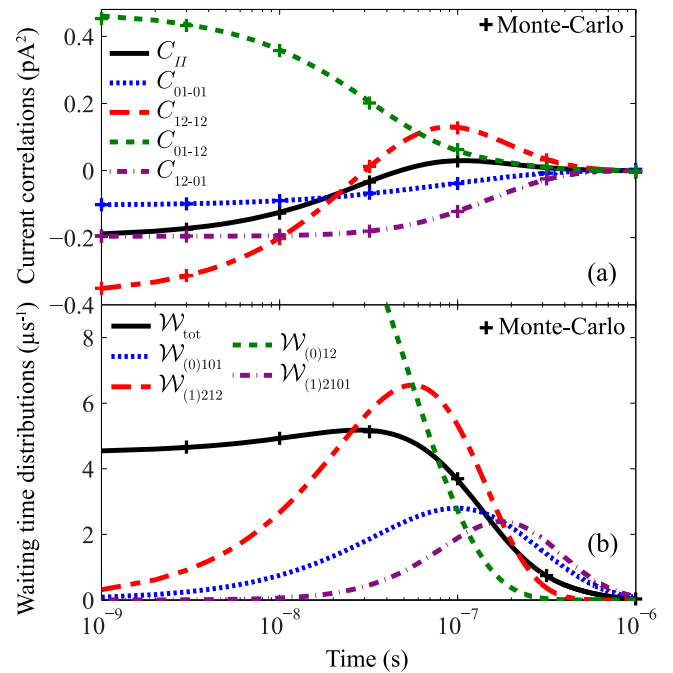

Figure 6. (a) Auto- and cross-correlations and (b) waiting time distributions corresponding to basic path and of the total current as a function of time in the case of Fano factor $F = 1.04$ ($V = 1.02$ V) in the 3-state case. The lines correspond to analytic results, the crosses are the results obtained using a Monte-Carlo algorithm.

unlikely to have two consecutive $0 \rightarrow 1$ ($1 \rightarrow 2$) pulses with low delay time, and auto-correlations C_{01-01} and C_{12-12} are negative. The same behavior is observed for cross-correlations C_{12-01} between $1 \rightarrow 2$ pulses and their following $0 \rightarrow 1$
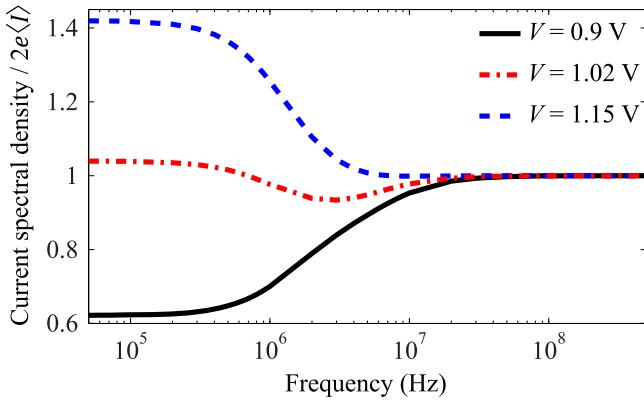
Figure 7. Current spectral density normalized by the value of a Poissonian process as a function of frequency for three different regimes.

pulses. Their absolute values at low time delays are linked with the probability of current pulses.

In the case where the minimum of Fano factor $F = 0.62$ is found, plotted in figure 4, current pulses $1 \rightarrow 2$ provide 84% of the total current (70% + 14%, see table 1). This reinforces the negative contribution of C_{12-12}, while C_{01-01} is close to zero, the value of C_{12-01} being always located between those two auto-correlations. As a consequence, the global auto-correlation function C_{II} is always negative before tending to zero, typical of a sub-Poissonian Fano factor.

On the contrary, $0 \rightarrow 1$ pulses (52%) contribute slightly more than the $1 \rightarrow 2$ ones (48%) at the maximum of Fano factor shown in figure 5. The 'weak' negative contributions of auto-correlations C_{01-01} and C_{12-12}, as well as C_{12-01}, are not sufficient to compensate the positive contribution of C_{01-12}, and the global auto-correlation function C_{II} is always positive, sign of a super-Poissonian zero-frequency SN.

In all the cases, the correlations C_{01-01}, C_{12-12} and C_{12-01} increase in parallel with their corresponding WTD until their maximum. This increase can lead the auto-correlations C_{12-12} around the maximum of $\mathcal{W}_{(1)212}$ to go from negative to positive values, as seen on cases $F = 1.15$ and $F = 1.04$ in figures 5 and 6, respectively: while Coulomb blockade provides a negative contribution for C_{12-12} at low delay times, the high probability to have two consecutive events during a time around which the WTD is maximum leads to a positive correlation for such values of the delay time. Remarkably, in the case of a nearly Poissonian Fano factor shown in figure 6, this behavior causes a global auto-correlation C_{II} to also switch from negative to positive values.

Finally, both WTDs and correlation functions vanish for long times. However, we have to notice that at long times the time-dependence of correlation functions and their corresponding WTDs are slightly different, as the WTDs concern only two consecutive pulses, while the correlations take into account any tunnel event with another, not only the consecutive ones. Therefore the correlation functions tend to disappear for longer times than WTDs. The path (1)2101 is the slowest of basic paths since it involves three events, hence

the maximum of $\mathcal{W}_{(1)2101}$ is located for higher time delays than $\mathcal{W}_{(1)212}$ and $\mathcal{W}_{(0)101}$.

The spectral densities corresponding to the previously discussed auto-correlation functions are plotted in figure 7. The spectral densities are equal to the zero-frequency value at low frequency before tending to the Poissonian value at high frequencies. In the case $V = 1.02\,\mathrm{V}$ ($F = 1.04$), studied in figure 6, we can clearly distinguish two regimes depending on the frequency, i.e. super-Poissonian at low frequencies, and sub-Poissonian in the $[10^6$–$10^7\,\mathrm{Hz}]$ range. This behavior is the direct consequence of the time-dependence behavior of the global auto-correlation function C_{II}, explained previously: negative for low delay times and then positive for intermediate values.

Additionally, we should notice that figures 4–6 show that the MC algorithm leads to the very same results as the analytic model for the 3-state case. This method offers the time-evolution of the number of electrons in the dot, and then of all tunnel events, based only on tunnel transfer rates, for any device. Indeed, this MC algorithm has previously shown its robustness for current calculation in different single-electron devices [57, 59, 60]. The MC method may be a good tool to understand the behavior of SN in case of more complex devices, hard to model analytically, such as the study of the real DTJ at finite temperature, including all basic paths depending on the number of states available, and also of double-dot structures, accounting for phonon scattering mechanisms.

4. Conclusion

Thanks to the ability of SENS code to provide tunnel transfer rates depending on the number of electrons in a QD, we have been able to calculate both the zero-frequency and the frequency-dependent SN in a given DTJ, and to separate it into different contributions, related to the basic paths followed by the system between two current pulses. The probabilities of these basic paths and the WTD statistical tool offer a clear understanding of current auto-correlation functions, and by extension of spectral densities, in both sub and super-Poissonian regimes. In particular, the remarkable behavior of a spectral density going from super to sub-Poissonian depending on the frequency is explained as a trade-off between high probability of a given basic path and high WTD for a given time range. Finally, the possibility of simulating more complex single-electron structures is open, thanks to the possibility to use a MC algorithm, instead of an analytic formalism of correlation functions.

Acknowledgments

References

[1] Landauer R 1998 *Nature* **392** 658–9

[2] Blanter Y and Büttiker M 2000 *Phys. Rep.* **336** 1–166

[3] Blanter Y 2005 *Recent Adv. Stud. Curr. Noise* (preprint cond-mat/0511478)

[4] Esposito M, Harbola U and Mukamel S 2009 *Rev. Mod. Phys.* **81** 1665–702

[5] Nazarov Y V 2003 *Quantum Noise in Mesoscopic Physics* (Berlin: Springer)

[6] Nazarov Y V and Blanter Y M 2009 *Quantum Transport: Introduction to Nanoscience* (Cambridge: Cambridge University Press)

[7] Averin D and Likharev K 1986 *J. Low Temp. Phys.* **62** 345–73

[8] Likharev K 1987 *IEEE Trans. Magn.* **23** 1142–5

[9] Likharev K 1999 *Proc. IEEE* **87** 606–32

[10] Takahashi Y, Ono Y, Fujiwara A and Inokawa H 2002 *J. Phys.: Condens. Matter* **14** R995

[11] Deshpande V *et al* 2013 *Solid-State Electron.* **84** 179–84

[12] Lee S, Lee Y, Song E B and Hiramoto T 2014 *Nano Lett.* **14** 71–7

[13] Shin S J, Jung C S, Park B J, Yoon T K, Lee J J, Kim S J, Choi J B, Takahashi Y and Hasko D G 2010 *Appl. Phys. Lett.* **97** 103101

[14] Shin S J, Lee J J, Kang H J, Choi J B, Yang S R E, Takahashi Y and Hasko D G 2011 *Nano Lett.* **11** 1591–7

[15] Tanahashi Y, Suzuki R, Saraya T and Hiramoto T 2014 *Japan. J. Appl. Phys.* **53** 04EJ08

[16] Bomze Y, Gershon G, Shovkun D, Levitov L S and Reznikov M 2005 *Phys. Rev. Lett.* **95** 176601

[17] Bylander J, Duty T and Delsing P 2005 *Nature* **434** 361–4

[18] Choi T, Ihn T, Schön S and Ensslin K 2012 *Appl. Phys. Lett.* **100** 072110

[19] Flindt C, Fricke C, Hohls F, Novotný T, Netočný K, Brandes T and Haug R J 2009 *Proc. Natl Acad. Sci. USA* **106** 10116–9

[20] Fricke C, Hohls F, Wegscheider W and Haug R J 2007 *Phys. Rev. B* **76** 155307

[21] Fujisawa T, Hayashi T, Tomita R and Hirayama Y 2006 *Science* **312** 1634–6

[22] Gershon G, Bomze Y, Sukhorukov E V and Reznikov M 2008 *Phys. Rev. Lett.* **101** 016803

[23] Gustavsson S, Leturcq R, Simovič B, Schleser R, Ihn T, Studerus P, Ensslin K, Driscoll D C and Gossard A C 2006 *Phys. Rev. Lett.* **96** 076605

[24] Gustavsson S, Leturcq R, Simovič B, Schleser R, Studerus P, Ihn T, Ensslin K, Driscoll D C and Gossard A C 2006 *Phys. Rev. B* **74** 195305

[25] Lu W, Ji Z, Pfeiffer L, West K W and Rimberg A J 2003 *Nature* **423** 422–5

[26] Mahé A, Parmentier F D, Bocquillon E, Berroir J M, Glattli D C, Kontos T, Plaçais B, Fève G, Cavanna A and Jin Y 2010 *Phys. Rev. B* **82** 201309

[27] Maisi V F, Kambly D, Flindt C and Pekola J P 2014 *Phys. Rev. Lett.* **112** 036801

[28] Pekola J P, Saira O P, Maisi V F, Kemppinen A, Möttönen M, Pashkin Y A and Averin D V 2013 *Rev. Mod. Phys.* **85** 1421–72

[29] Sukhorukov E V, Jordan A N, Gustavsson S, Leturcq R, Ihn T and Ensslin K 2007 *Nat. Phys.* **3** 243–7

[30] Ubbelohde N, Fricke C, Flindt C, Hohls F and Haug R J 2012 *Nat. Commun.* **3** 612

[31] Watase N, Hashisaka M, Muraki K and Fujisawa T 2014 *Japan. J. Appl. Phys.* **53** 04EJ01

[32] Zhang X C, Mazzeo G, Brataas A, Xiao M, Yablonovitch E and Jiang H W 2009 *Phys. Rev. B* **80** 035321

[33] Levitov L and Lesovik G 1993 *JETP Lett.* **58** 230

[34] Levitov L S, Lee H and Lesovik G B 1996 *J. Math. Phys.* **37** 4845–66

[35] Bagrets D A and Nazarov Y V 2003 *Phys. Rev. B* **67** 085316

[36] Korotkov A N 1994 *Phys. Rev. B* **49** 10381–92

[37] Birk H, de Jong M J M and Schönenberger C 1995 *Phys. Rev. Lett.* **75** 1610–3

[38] Hershfield S, Davies J H, Hyldgaard P, Stanton C J and Wilkins J W 1993 *Phys. Rev. B* **47** 1967–79

[39] Belzig W 2005 *Phys. Rev. B* **71** 161301

[40] Cottet A and Belzig W 2004 *Europhys. Lett.* **66** 405

[41] Cottet A, Belzig W and Bruder C 2004 *Phys. Rev. B* **70** 115315

[42] Ubbelohde N, Fricke C, Hohls F and Haug R J 2013 *Phys. Rev. B* **88** 041304

[43] Sukhorukov E V, Burkard G and Loss D 2001 *Phys. Rev. B* **63** 125315

[44] Emary C, Marcos D, Aguado R and Brandes T 2007 *Phys. Rev. B* **76** 161404

[45] Marcos D, Emary C, Brandes T and Aguado R 2011 *Phys. Rev. B* **83** 125426

[46] Albert M, Flindt C and Büttiker M 2011 *Phys. Rev. Lett.* **107** 086805

[47] Albert M, Haack G, Flindt C and Büttiker M 2012 *Phys. Rev. Lett.* **108** 186806

[48] Albert M and Devillard P 2014 *Phys. Rev. B* **90** 035431

[49] Brandes T 2008 *Ann. Phys., Lpz.* **17** 477–96

[50] Haack G, Albert M and Flindt C 2014 *Phys. Rev. B* **90** 205429

[51] Rajabi L, Pöltl C and Governale M 2013 *Phys. Rev. Lett.* **111** 067002

[52] Tang G M, Xu F and Wang J 2014 *Phys. Rev. B* **89** 205310

[53] Thomas K H and Flindt C 2014 *Phys. Rev. B* **89** 245420

[54] Thomas K H and Flindt C 2013 *Phys. Rev. B* **87** 121405

[55] Welack S, Esposito M, Harbola U and Mukamel S 2008 *Phys. Rev. B* **77** 195315

[56] Welack S, Mukamel S and Yan Y 2009 *Europhys. Lett.* **85** 57008

[57] Sée J, Dollfus P and Galdin S 2006 *IEEE Trans. Electron Devices* **53** 1268–73

[58] Sée J, Dollfus P, Galdin S and Hesto P 2006 *J. Comput. Electron.* **5** 35–48

[59] Valentin A, Galdin-Retailleau S and Dollfus P 2009 *J. Appl. Phys.* **106** 7

[60] Talbo V, Galdin-Retailleau S, Valentin A and Dollfus P 2011 *IEEE Trans. Electron Devices* **58** 3286–93

[61] Talbo V, Querlioz D, Retailleau S and Dollfus P 2012 *Fluctuation Noise Lett.* **11** 1242006

[62] Sée J, Dollfus P and Galdin S 2002 *Phys. Rev. B* **66** 193307

[63] Sée J, Dollfus P and Galdin S 2002 *J. Appl. Phys.* **92** 3141–6

[64] Bardeen J 1961 *Phys. Rev. Lett.* **6** 57–9